The D-wave to S-wave amplitude ratio for $b_1^-(1235) \to \omega\pi^-$

Mina Nozar[a]

[a]Department of Physics, Applied Physics and Astronomy
Rensselaer Polytechnic Institute
Troy, NY, 12180-3590 USA

We present a preliminary measurement of D/S amplitude ratio in $b_1^- \to \omega\pi^-$. Events are selected from experiment $E852$ [1] at BNL, using $\pi^- p \to \omega\pi^- p$, $\omega \to \pi^+\pi^-\pi^0$. The $\omega\pi^-$ mass spectrum is dominated by $b_1(1235)$ and $\rho_3(1690)$. Partial Wave Analysis (PWA) was used to determine D/S. A separate PWA of the ω-sideband events was used to determine background. We find a preliminary D/S value of 0.327 ± 0.013, where the error is statistical only. The total error, however, is dominated by the systematic uncertainties, currently under study.

1. Introduction

In the quark model, the $b_1(1235)$ meson is well described as a $q\bar{q}$ pair with total spin $S = 0$, orbital angular momentum $L = 1$, and isospin $I = 1$ [2]. Its dominant decay mode is $b_1 \to \omega\pi$. This decay is possible and has been observed in an $l = 0\,(S - wave)$ or $l = 2\,(D - wave)$, where l is the relative angular momentum between ω and π.

Previous measurements [4] yield a wide range of values (see Table 1). The Particle Data Group (PDG) recommends 0.29 ± 0.04, an average of the values listed in the table.

Table 1
D/S measurements as listed in PDG

Experiment	Year	Reaction	Beam Energy (GeV)	D/S
CBAR	1994	$\bar{p}p \to \omega\eta\pi^0$	0.0	0.23 ± 0.03
	1993	$\bar{p}p \to \omega\pi^0\pi^0$	0.0	0.45 ± 0.04
OMEG	1984	$\gamma p \to \omega\pi^0 p$	$20 - 70$	0.235 ± 0.047
HBC	1977	$\pi^- p \to \omega\pi^- p$	11	0.4 ± 0.1
	1975	$\pi^+ p \to \omega\pi^+ p$	7.1	0.21 ± 0.08
	1974	$\pi^- p \to \omega\pi^- p$	$3.9 - 7.5$	0.3 ± 0.1
	1974	$\pi^+ p \to \omega\pi^+ p$	4.9	0.35 ± 0.25

Accurate measurements of certain amplitude ratios such as the D-wave to S-wave ratio (D/S) in $b_1 \to \omega\pi$ and $a_1 \to \rho\pi$ are important tests for strong hadronic decay models [3]. Fig. 1 shows the prediction for the two leading models, $^3P_0$ and $^3S_1$. An amplitude ratio analysis is more sensitive to the decay dynamics than to the hadronic structure of the b_1.

2. Data Selection

The data for this analysis was collected in the 1995 run of E852, using the Multi-Particle Spectrometer (MPS) [5] facility at Brookhaven National Laboratory. The MPS was augmented by a cylindrical wire chamber (TCYL) [6] around the target for detection of charged recoils, a 198-element cylindrical Cesium Iodide (CsI) [7] detector around TCYL

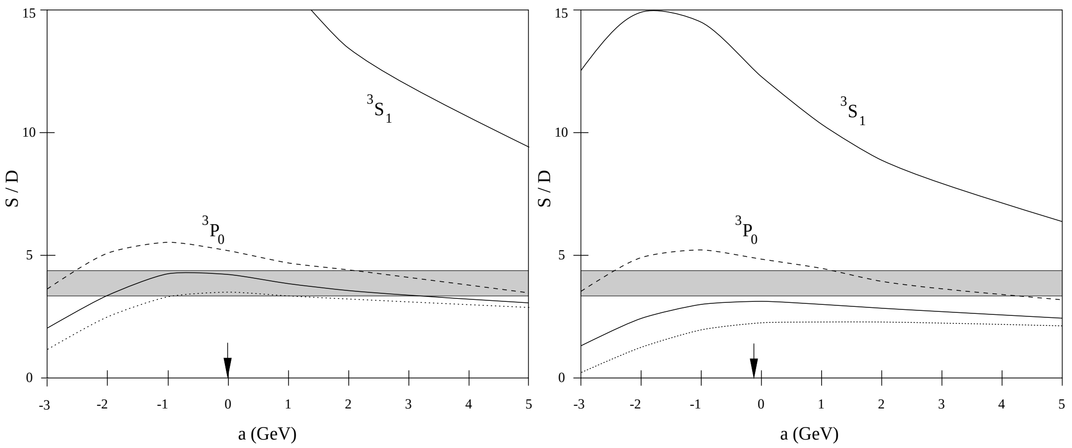

Figure 1. S/D amplitude ratio for $b_1 \rightarrow \omega\pi$ as a function of FSI strength a for various wave function and various flux-tube choices. In the left graph, SHO wave functions were used; in the right,Coulomb-plus-linear wavefunctions. Dashed lines show narrow flux-tube results, solid lines show medium flux-tube results, dotted lines show wide flux-tub results. (In the $^3S_1$ model, there is negligible dependence on the type of flux tube, so only a solid line is shown.) The arrows indicate Geiger and Swanson's estimates of the actual FSI strengths. The shaded bands give the experimental ratios.

to veto soft photons, a downstream 2-plane drift chamber (TDX4) to help track reconstruction, and a 3045-element lead glass calorimeter (LGD) [8] for detection of neutrals. Two proportional wire chambers (TPX1-2) interspersed between six seven-plane drift chambers (DC1-6) [9] inside the MPS magnet, provided a forward multiplicity trigger. We recorded $265M$ triggers with three forward going charged particles and one charged recoil. After requiring charge, energy and momentum conservation, and topological cuts, 8.2 million events of the type $\pi^+\pi^-\pi^-\gamma\gamma$ remained. A 2-C kinematical fit, requiring a proton recoil at the main vertex and a π^0 from the 2γ's, resulted in $1.2M$ $\pi^+\pi^-\pi^0\pi^-$ events, with a confidence level (c.l.)$> 5\%$. We imposed an additional kinematical constraint that the $\pi^+\pi^-\pi^0$ form a narrow ω, imposed. Choosing events with c.l. $> 5\%$, a final sample of $224K$ $\omega\pi^-p$ events remained. Fig. 2 shows the $\pi^+\pi^-\pi^0$ and $\omega\pi^-$ mass spectra.

An expansion of the (3π) mass distribution near the ω is shown in in Fig. 3a. It is possible to estimate background level under the ω-peak using ω-sideband events; however, its is wrong to assume that the background events have "flat" angular distributions. In fact, ω-sideband events show "non-flat" angular distributions. The decay matrix element in $\omega \rightarrow \pi^+\pi^-\pi^0$ can be written in the ω rest frame as: [10]

$$\lambda = \frac{|\vec{p}_{\pi^+} \times \ \vec{p}_{\pi^-}|^2}{|\vec{p}_{\pi^+} \times \ \vec{p}_{\pi^-}|^2{}_{max}}$$

This description gave us a handle on estimating the non-ω $\pi^+\pi^-\pi^0$ events under the ω peak. The background to signal ratio is on the order of 29%. This background consists of events with the triplet $\pi^+\pi^-\pi^0$ mass in the ω region but not in a $J^p = 1^-$ state. A quantitative way of measuring the number of true ω's is by treating $\omega \rightarrow 3\pi$ as a two body decay through a mediary virtual two-body system and looking at the angle between the bachelor pion and one of the pions from the decay of the two-body system in its rest system. This distribution in $\cos(\theta_h^*)$ as a $\sin^2(\theta_h^*)$ shape for ω events and a linear shape for the background events. By extracting the number of true ω's from all events in the ω

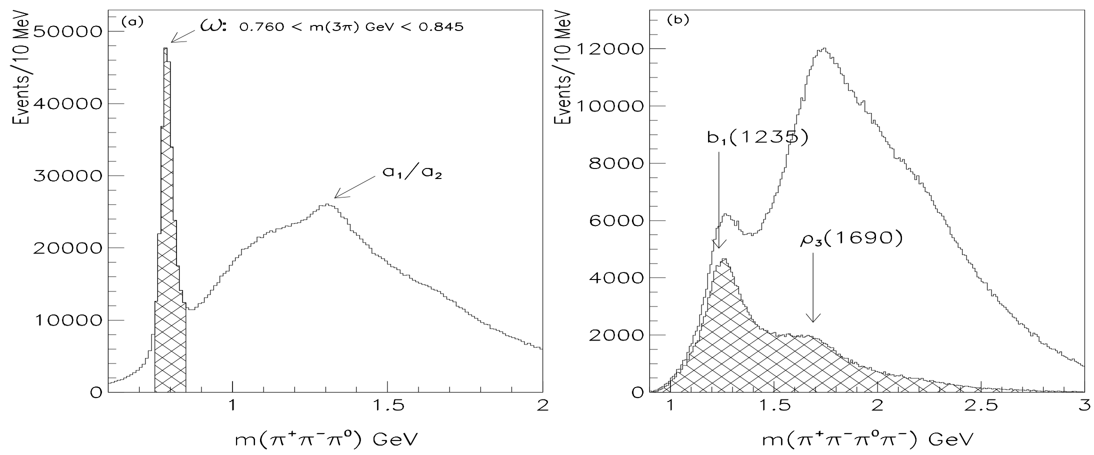

Figure 2. Effective mass spectra: (a) $\pi^+\pi^-\pi^0$ effective mass. (b) $\pi^+\pi^-\pi^0\pi^-$ and $\omega\pi^-$ effective mass. The hatched regions correspond to an ω mass cut.

region, we can look at any given distribution in the data from true ω contribution. This method has successfully been used before [11]. Fig. 3 also shows $\cos(\theta_h^*)$ distribution for events in the ω peak region and for the events in the ω sideband region. We also show the $\omega\pi^-$ spectrum before and after weighting the events by $[-C \times Y_2^0(\theta_h^*)]$, where C is a normalization constant.

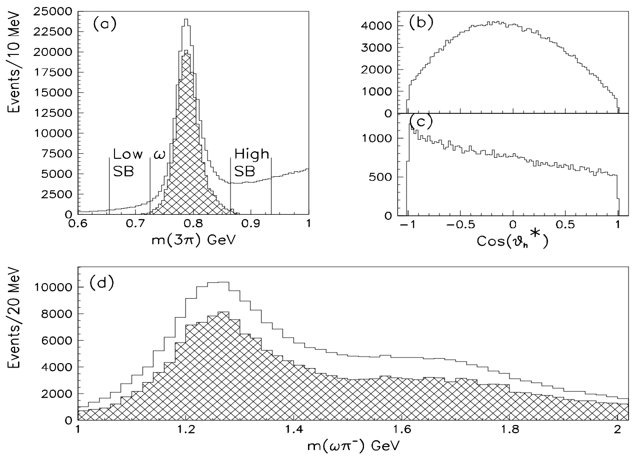

Figure 3. (a) $\pi^+\pi^-\pi^-$ effective mass distribution before and after weighting by $[-C \times Y_2^0(\theta_h^*)]$. (b) $\cos(\theta_h^*)$ for events in the ω peak region. (c) $\cos(\theta_h^*)$ for events in the ω low and high sideband regions. (d) $\omega\pi^-$ effective mass distribution before and after weighting by $[-C \times Y_2^0(\theta_h^*)]$.

3. PWA results

For details of the PWA formalism used by the $E852$ collaboration, the reader is referred elsewhere [12,13]. Numerous fits were performed on the $224K$ $\omega\pi^-$ events with varying numbers of input waves, different $\omega\pi^-$ mass bin widths, different regions in t and different description of the background term. Fig. 3 shows the result of one PWA fit in $60MeV$ mass bin with $-t$ in the range: $0.1 \leq -t \leq 5$ $(GeV/c)^2$. The fit included 1^{+-}, 3^{--}, 1^{--} waves and a non-interfering isotropic background term. Clear structure is observed in the 1^{+-} wave in the b_1 region. The 3^{--} wave is dominated by ρ_3. The 1^{--} wave shows an enhancement in the $1250 - 1300\ MeV$ mass region. In Fig. 5, we show all contributions to the 1^{+-} wave separately. The b_1 is produced mostly in the positive reflectivity, $\epsilon = +$, which implies natural parity exchange, namely ω.

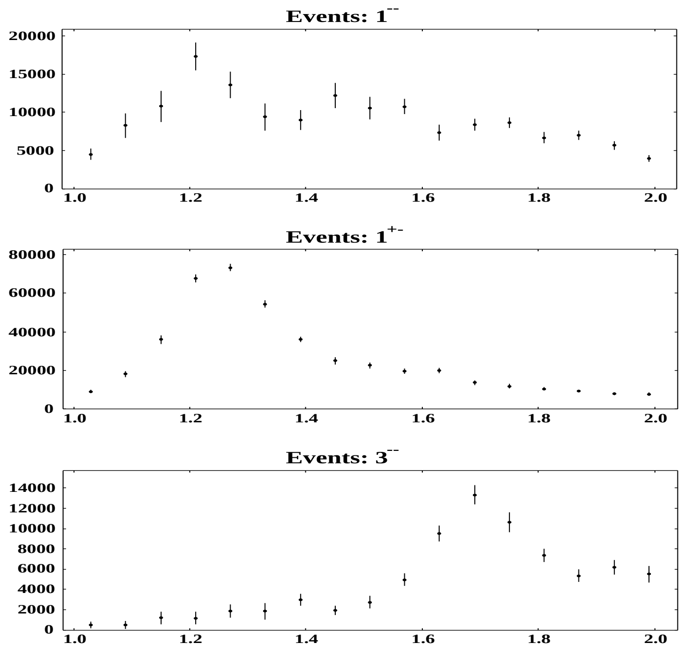

Figure 4. PWA fit result for the $\omega\pi^-$ system. The plot shows intensities for the following waves: top: 1^{+-}, middle: 3^{--}, bottom: 1^{--}. Intensities are plotted as a function of $\omega\pi^-$ mass in GeV/c.

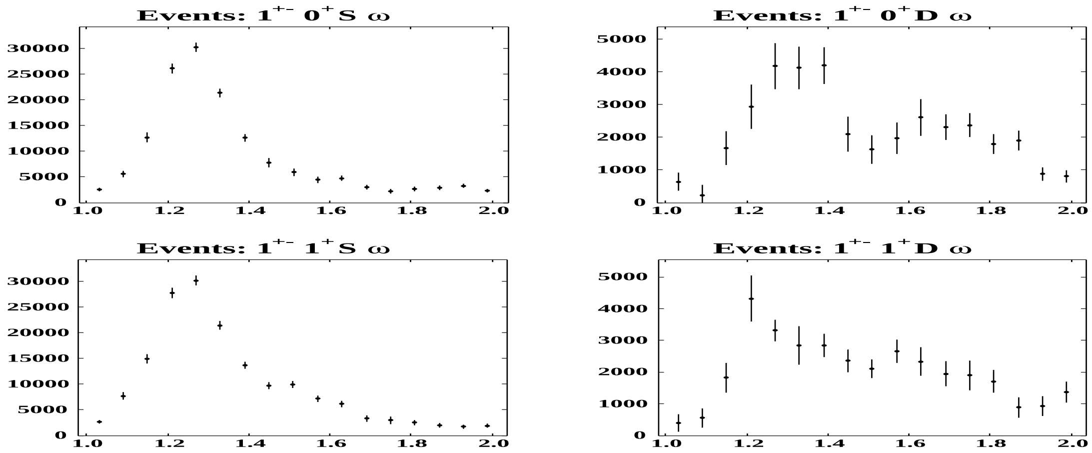

Figure 5. PWA fit result for 1^{+-} wave. The left and right columns shows possible S-wave and D-wave amplitudes respectively. M^ϵ is 0^+ for the top plot and 1^+ for the bottom plot. Intensities are plotted as a function of $\omega\pi^-$ mass in GeV/c.

For the first set of fits, we used waves including only ω as a stable isobar and a "flat" non-interfering background term. At this point, we noticed a discrepancy between the signal to background ratio from the results of the PWA and the ω extraction method mentioned earlier. Fig. 6 shows the difference. The PWA results showed a higher signal to background ratio. In the process of understanding the background events, we discovered that the angular distributions of the ω-sideband events were not "flat", we therefore, needed more than a non-interfering "flat" term in the PWA to account for this background. Since the predicted angular distributions from the PWA fit results to the ω-sideband events using only $a_1(1260)$ and $a_2(1320)$ isobars were in reasonable agreement with the data, our first attempt was to include these isobars in the PWA fits to the $\omega\pi^-$ events. In general, other isobars such as ρ and $(\pi\pi)_s$ would be needed to describe the background completely. Inclusion of the waves with a_1 and a_2 isobars, helped us achieve better agreement in the signal to background ratio as shown in Fig. 6.

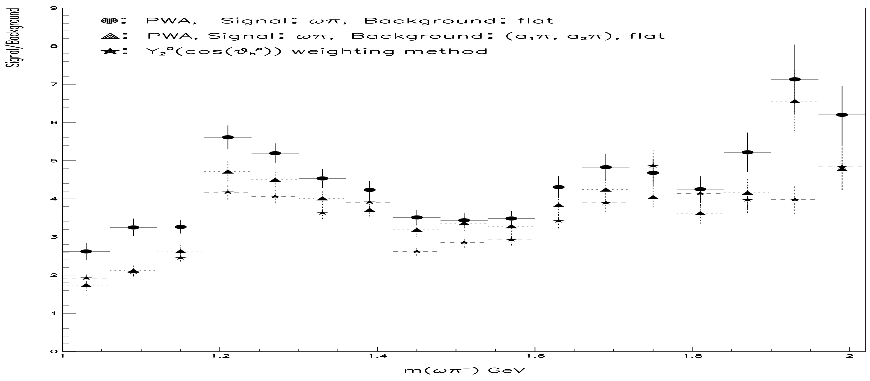

Figure 6. Signal to Background as a function of $\omega\pi^-$ mass.

4. D/S amplitude ratio measurement technique

In measuring the D/S amplitude ratio, we started with a PWA fit for a $100MeV$ wide bin around the b_1 mass, using both the D and S waves. In the subsequent fits, the D waves were taken out and the combined amplitude, $S + \alpha \times S$ replaced the original S wave amplitudes, where α was taken to be a complex number, whose real part represents the D/S amplitude ratio and its imaginary part represents the phase difference between the S and D waves. We scanned the fits over the α magnitude, with its phase fixed at zero, then for the α-magnitude which gave us a minimum $ln(likelihood)$ value, scanned over the α-phase. Fig. 7 shows the results of one such scan. From the figure, it is clear that the statistical error is very small.

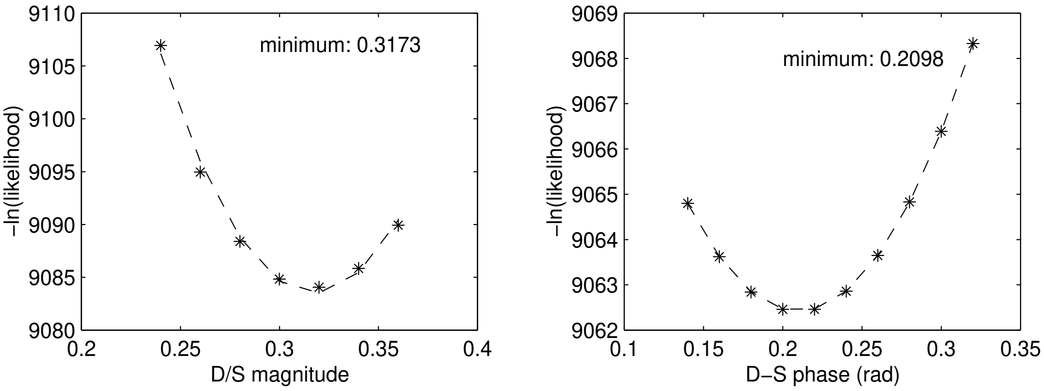

Figure 7. Results of a scan over α-magnitude (D/S ratio) and α-phase ($D - S$) phase difference.

5. Work in progress

As mentioned before, the error in our measurement of the $b_1 \rightarrow \omega\pi$ D/S amplitude ratio measurement is dominated by systematic uncertainties. We still need to understand which variables our measurement is most sensitive to (i.e. set of waves used in the fits, the rank of the fit, etc). We also need to determine whether our description of the background term is sufficient. We will repeat PWA fits in finer $\omega\pi^-$ mass bins to study the D/S fluctuations over the b_1 mass range. Performing fits in t bins may provide insight as to which waves to include in the fits around the b_1 mass. We will also investigate the structure in the $J^{pc} = 1^{--}$ wave.

REFERENCES

1. The BNL-E852 collaboration consists of BNL, IHEP (Protvino/Russia), Indiana U., U. Mass.(Dartmouth), Moscow State U., Northwestern U., Notre Dame U., and RPI.
2. Stephen Godfrey and Nathan Isgur *Mesons in a relativized quark model with chromodynamics*, *Phys. Rev.* **D32**, 189-231 (1985).
3. Paul Geiger, Eric S. Swanson, *Distinguishing among strong decay models*, *Phys. Rev.* **D50**, 6855-6862 (1994).
4. C. Caso et al., The European Physical Journal **C3**, 379 (1998).
5. S. Ozaki, “Abbreviated Description of the MPS”, Brookhaven MPS note 40 (1978). unpublished. the MPS”, Brookhaven MPS note 40, unpublished (1978).
6. Z. Bar-Yam et al., Nucl. Instr. & Meth. A **386**, 235 (1997).
7. T. Adams et al., Nucl. Instr. & Meth. A **368**, 617 (1996).
8. R.R. Crittenden et al., Nucl. Instr. & Meth. A **387**, 377 (1997).
9. S.E. Eiseman et al., Nucl. Instr. & Meth. **217**, 140 (1983).
10. C. Zemach, *Three-Pion Decays of Unstable Particles*, *Phys. Rev.* **133**, B1201 (1964).
11. Youngjoon Kwon, P.h.D. Thesis: *Strange Meson Spectroscopy in $K\omega$ and $K\phi$ at 11 GeV/c and Cherecnkov Ring Imaging at SLD*, SLAC-409 (1993).
12. J.P. Cummings and D.P. Weygand, BNL-64637.
13. S.U. Chung and T.L. Trueman, Phys. Rev. **D11**, 633(1975).